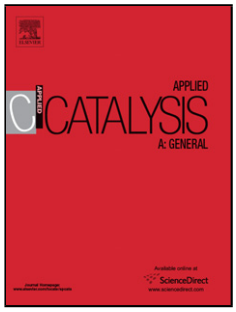

Title: Mono and bimetallic Cu-Ni structured catalysts for the water gas shift reaction

Author: O. Arbeláez T.R. Reina S. Ivanova F. Bustamante A.L. Villa M.A. Centeno J.A. Odriozola

PII: S0926-860X(15)00139-8
DOI: http://dx.doi.org/doi:10.1016/j.apcata.2015.02.041
Reference: APCATA 15283

To appear in: *Applied Catalysis A: General*

Received date: 1-11-2014
Revised date: 20-1-2015
Accepted date: 23-2-2015

Please cite this article as: O. Arbeláez, T.R. Reina, S. Ivanova, F. Bustamante, M.A. Centeno, J.A. Odriozola, Mono and bimetallic Cu-Ni structured catalysts for the water gas shift reaction, *Applied Catalysis A, General* (2015), http://dx.doi.org/10.1016/j.apcata.2015.02.041

Mono and bimetallic Cu-Ni structured catalysts for the water gas shift reaction

O. Arbeláez[1], T.R. Reina[2]*, S. Ivanova[2], F. Bustamante[1]*, A.L.Villa[1], M.A. Centeno[2], J. A. Odriozola[2]

[1]Environmental Catalysis Research Group, Chemical Engineering Department, Engineering Faculty, Universidad de Antioquia UdeA, Calle 70 No. 52-21, Medellín, Colombia

[2]Departamento de Química Inorgánica e Instituto de Ciencia de Materiales de Sevilla, Universidad de Sevilla-CISC Avda. Américo Vespucio 49, 41092, Spain

* Corresponding author: ***felipe.bustamante@udea.edu.co ; tomas.ramirez@icmse.csic.es***

Highlights

- Efficient Cu-Ni catalysts supported on activated carbon for the water gas shift reaction.
- Supressed methanation activity due to the presence of Cu.
- Cu-Ni alloy as a key factor of the catalytic design.
- Good stability and tolerance towards start/stop situations.

Abstract

The water-gas shift (WGS) reaction over structured Cu, Ni, and bimetallic Cu-Ni supported on active carbon (AC) catalysts was investigated. The structured catalysts were prepared in pellets form and applied in the medium range WGS reaction. A good activity in the 180-350 °C temperature range was registered being the bimetallic Cu-Ni:2-1/AC catalyst the best catalyst.

The presence of Cu mitigates the methanation activity of Ni favoring the shift process. In addition the active carbon gasification reaction was not observed for the Cu- containing catalyst converting the active carbon in a very convenient support for the WGS reaction. The stability of the bimetallic Cu-Ni:2-1/AC catalyst under continuous operation conditions, as well as its tolerance towards start/stop cycles was also evaluated.

Key words: water gas shift, pelletized catalyst, activated carbon, Cu-Ni catalyst

1. Introduction

The demand for high-purity hydrogen is rapidly growing in the electronic and chemical industry, especially in the ammonia and methanol synthesis [1]. Recently, there has been an increasing interest in using hydrogen as a clean fuel in gas turbines or fuel-cells for power generation. Hydrogen is considered as the "green fuel of the future" and a promising alternative to oil and natural gas as energy carriers and prime movers [2]. All these applications demand high-purity H_2, i.e., with trace amounts of CO impurities. For example, CO levels below 10 ppm are required for fuel cells applications and 5 ppm is the acceptable limit for the ammonia synthesis [3]. Commercially, natural gas steam reforming is the most employed way to produce hydrogen, where the resulting reformate gas contains 10−13 vol. % CO [4]. After the reforming units, water gas shift (WGS) reactors reduced the carbon monoxide to 1-2% subsequently treated to trace levels either by the preferential CO oxidation in the presence of H_2 (PROX) [5] units, or selective methanation of CO reactors [6] before delivering H_2 for the end-user applications.

The water gas shift reaction (eq.1) allows the conversion of carbon monoxide and water to hydrogen and carbon dioxide; the WGS is an exothermic, equilibrium process (ΔH= - 41.1 kJ/mol), [7].

$$\mathbf{CO + H_2O \leftrightarrow CO_2 + H_2} \quad \text{Eq. 1}$$

A large number of noble metal based catalysts, such as Pd-Zn/CeO_2 [8], Pd-Zn [9], Pd-$LaCoO_3$ [10], Pt-ZrO_2 [11], Pt-TiO_2 [12], Pt-CeO_2 [13], Au-CeO_2 [14] and Au-Al_2O_3 [15], have been reported to be effective for this reaction. Nevertheless, Pt [16], Pd [7] and Au [17] supported catalysts used under realistic water gas shift streams and in frequent start/stop cycles are irreversibly deactivated. Furthermore, the destabilization at high temperatures by sintering of the metal and support has also been reported and represents a problem to overcome for the noble metal supported catalysts in the WGS [18]. Moreover, the high cost associated with Pd and Pt based catalysts is also considered as a serious drawback [19]. Therefore, one of the challenges of catalyst's design is the substitution of noble metals [20] with more common and less expensive alternatives while maintaining high catalytic efficiency. Cu, Ni and Cu-Ni supported on activated carbon has been used in methanol [21], dimethyl carbonate [22], and diethyl carbonate synthesis [23] and in principle are also suitable for the WGS reaction [24]. Nowadays, Cu and Ni metals supported on SiO_2 [25], Al_2O_3 [26], CeO_2 [27] and ZrO_2 [28], have been widely employed as heterogeneous catalysts for the water gas shift reaction. However, these catalysts have relatively low surface area and they are also deactivated under start/stop cycles. Recently, some studies have demonstrated that the activated carbon could be used as versatile support for transitions metals in catalytic heterogeneous reactions [29]. This material presents mechanical, chemical and thermal stability, electrical transporting properties, longevity, low cost and high surface area. However, an important drawback of carbon supported catalysts is their low mass thus implying the need of large amount of catalyst in the catalytic bed and the consequent problems of pressure drop. In this way, the use of carbon powders processed into pellets (cylindrically-shaped pieces) or monolithic geometries is mandatory to reduce the total catalyst volume, the pressure drop in

the catalytic bed, and the formation of hotspots. In a certain way the pelletized catalysts fill the gap between powder samples and monolith catalyst. An additional benefit of the application of pelletized catalysts is also their easy handling.

For all stated above, in this work, commercial activated carbon powder was pelletized and subsequently impregnated with copper and nickel resulting in Cu and Ni monometallic and bimetallic carbon supported catalysts. The prepared materials were tested in the WGS reaction using model and realistic conditions. The stability and the tolerance towards start/stop operations were analyzed for the most active catalyst to evaluate its feasibility for a real application.

2. Experimental Section

2.1 Catalysts preparation

Commercial activated charcoal (AC), Merck (90% particle size < 100 μm), was mixed with an ethanolic solution (10% weight) of carboxymethylcellulose (CMC) as a binder; the solution was stirred and heated softly for 24 h until ethanol evaporation. The remaining solid was wetted with water to form a paste, which was pressed in an uniaxial hydraulic system at 1 metric ton for 15 minutes. The compacted carbon was then extruded in cylindrical shape and cut in pellets (Ø 3.175 mm x 4 mm). After drying at 80 ºC for 12 h, the pellets were pyrolyzed for 3 hour at 600ºC in N_2 flow (25 mL/min) with a heating rate of 0.5 ºC/min and subsequently used as catalyst support.

The monometallic Cu, Ni and bimetallic Cu-Ni/AC catalysts were prepared by conventional wetness impregnation of the obtained pellets. $Cu(NO_3)_2 \cdot 3H_2O$ and $Ni(NO_3)_2 \cdot 6H_2O$ were used as metal precursors to obtain a nominal metal oxide (CuO + NiO) loading of 20 wt%. The Cu:Ni molar ratio was fixed to 2:1 and 1:2, respectively. After mixing of the precursor aqueous

solutions with the AC pellets, the mixture was roto-evaporated at reduced pressure for 3 h. The pellets were then dried at 90 ºC for 12 h and heated in flowing N_2 (25 mL/min) at 0.5 ºC/min up to 500 ºC and held for 3 h. Then, the solid was reduced in 5% H_2/Ar at 600 ºC during 3 h with 0.5 ºC/min heating rate. After reduction no additional precaution were employed for catalyst's storage.

2.2. Catalysts characterization

2.2.1 X-Ray diffraction

The crystallinity and the phase composition of the synthesized materials was determined by X-ray diffraction (XRD) on a Phillips PW 1740 diffractometer using Cu Kα radiation and Ni filter operated at 40 kV and 20 mA at room temperature. The scanning range was 2θ = 5-70° at 2°/min. The obtained diffractograms were compared to those of known compounds taken from JCPDS (Joint Committee of Powder Diffraction Standards) index.

2.2.2 BET measurements

Nitrogen adsorption/desorption isotherms were measured by nitrogen adsorption at liquid nitrogen temperature (77 K) using a Micromeritics Tristar II apparatus. The Brunauer-Emmett-Teller (BET) and the Barret-Joyner-Halenda approaches were used to determine the surface area and the pore size distribution of samples, respectively. Before analysis, the samples were degassed at 150 °C in vacuum during 2 h.

2.2.3 X-Ray microfluorescence spectrometry

The metallic loadings of the monometallic and bimetallic samples were determined by X-Ray microfluorescence spectrometry (XRMF) in an EDAX Eagle III spectrophotometer with a rhodium source of radiation working at 40 KV.

2.2.5 Temperature Programmed Desorption

Temperature-programmed desorption (TPD) experiments of the pre- and post WGS reaction samples were performed in a homemade apparatus coupled to a mass spectrometer Thermostar-QMS 200, Pfeiffer Vacuum. The m/e ratios in the 2-60 range were registered but only m/e = 2 (H_2), m/e = 18 (H_2O), m/e = 28 (CO) and m/e = 44 (CO_2) signal were detected and represented. 80 mg of the samples were heated in 25 mL/min flowing argon up to 900 °C at 10 ° C/min.

2.2.6. Temperature Programmed reduction TPR

H_2-TPR experiments of the reduced catalyst samples were performed in a Micromeritics AutoChem II 2920 apparatus. 100 mg samples were pretreated at 5°C/min to 250 °C for 1 h in flowing helium (70 mL/min), and then cooled to 40 °C. Thereafter, samples were heated to 800 °C using 5% H_2/Ar (70 mL/min) at 8 °C/min. The signals of H_2 consumption were continuously monitored by a thermal conductivity detector (TCD). For quantitative analysis the experimental H_2 consumption was compared to that of known weight of CuO (99.999%) standard.

2.2.7 X-ray photoelectron spectroscopy XPS

Surface properties of Cu, Ni and Cu:Ni-2:1 catalysts were investigated by X-ray photoelectron spectroscopy (XPS). XPS was performed with a Thermo VG Scientific Escalab 250 spectrometer equipped with a hemispherical electron analyzer and an Al Kα radiation source (1486.6 eV)

powered at 20 kV and 30 mA, respectively. The binding energy (BE) was determined by using carbon C (1s) line as reference with a binding energy of 284.6 eV. Peak fitting was done by using XPSPEAK 41 with Shirley background. High resolution core level scans were acquired from the surface of the freshly fractured catalysts for O 1s, C 1s, Cu 2p, and Ni 2p. Relative concentrations of the elements were determined from the integral intensities of the XPS peaks using the cross-sections according to Scofield.

2.3 Catalysts evaluation

The water gas shift reaction was carried out placing around 250 mg of catalyst (corresponding to 1.5 cm^3) in a continuous stainless steel tubular flow reactor (0.75 cm ID) operated at atmospheric pressure in the 180 - 350 ºC temperature range using two reaction feeds, named "model" and "realistic conditions". For the model WGS reaction just water and CO diluted in nitrogen were used, while for the realistic WGS reaction a reformate gas surrogate containing hydrogen and carbon dioxide was selected (Table 1). Water was injected into flowing gas stream by HPLC pump, and vaporized and homogenized with the gas feed before entering the reactor. Prior the catalytic measurements, the samples were treated under a 20 cm^3/min of H_2 for 30 min.

Table 1. Experimental conditions of the catalytic tests

	CO (vol%)	H_2O (vol %)	CO_2 (vol %)	H_2 (vol%)	N_2 (vol%)	Bed volume (cm^3)	GHSV (h^{-1})
Model	4.5	30.6	---	---	Balance	1.5	4000
Realistic	9	30.6	11	50	---	1.5	4000
Methanation	4	30	11	50	Balance	1.5	4000

The CO, CO_2 and water contents were analyzed with an ABB gas analyzer and the activity expressed in terms of CO conversion (X_{CO}) according to equation 2.

$$X_{CO} = \frac{\%CO_{in} - \%CO_{out}}{\%CO_{in}} * 100 \qquad \text{eq. 2}$$

Where % CO_{in} and % CO_{out} are the concentration of carbon monoxide at the inlet and outlet of the reactor, respectively. In addition, the methanation reaction was investigated to discern the CO consumption exclusively due to the shift process. For the methanation the reaction conditions were adjusted as closer as possible to the gas mixture contents of the realistic WGS mixture (Table 1). The products were analyzed using on-line gas chromatography in a Micro GC Varian equipped with MolSieve and Porapak columns. Methanation yield is expressed as follows:

$$CH_4 yield = \frac{CH_4 \ \ outlet}{CO \ \ inlet} * 100 \qquad \text{eq. 3}$$

3. Results and discussion

3.1 Catalytic results

3.1.1 Effect of the temperature in water gas shift reaction

The effect of the temperature on the catalytic activity for all the tested catalysts in the WGS reaction is presented in Figure 1.

Insignificant water gas shift activities were observed in the low temperature range (180 - 220 ºC). The monometallic Cu and Ni catalysts behave differently in this range. For the Ni containing

samples the production of carbon monoxide (negative conversion) was observed, which could be probably related to the carbon gasification reaction, namely the oxidation of carbon by steam to produce CO, CO_2 and H_2. This behavior was previously reported for supported Ni catalysts [30], one of the most active metal for the gasification of activated carbons at low temperatures.

Contrary to the Ni based sample, the Cu monometallic catalyst was not active in the low temperature range. In parallel, both bimetallic catalysts exhibited similar behavior to that of Cu monometallic one; no formation of CO is detected at low temperature indicating that the presence of Cu attenuates the gasification activity of Ni. At temperatures > 220 °C the CO conversion increased as a function of temperature (Figure 1). Interestingly, Cu-Ni:2-1/AC and Ni/AC samples demonstrated higher CO conversion at 350 ºC than Cu/AC and Cu-Ni:1-2/AC, (98.9% and 99.4% *vs.* 57.3% and 73.4 %, respectively). In comparison to the equilibrium CO concentration at this temperature (99.2%) the Ni/AC catalysts shows higher CO conversion which suggests the participation of other reactions. Taking into consideration that Ni containing catalysts are recognized as very efficient systems for methane production through CO hydrogenation reaction (eq. 5) [31], an increase of the CO consumption could be caused by CH_4 formation.

$$CO + 3\,H_2 \longrightarrow CH_4 + H_2O \qquad \text{eq. 5}$$

In order to clarify if there is some contribution of the methanation reaction to the observed CO conversion in the WGS, a methanation test was carried out. Figure 2 shows the catalytic activity (in terms of CH_4 yield) of all the tested samples.

The increase of the reaction temperature from 250 °C to 350 °C resulted in a continuous increase of the CH_4 yield. In Ni monometallic sample CH_4 yield reaches 14.7 % while in Cu-Ni:2-1 and Cu-Ni:1-2 bimetallic samples the maximum yield was 2.4 % and 1.3 %, whereas no CH_4 formation was observed for Cu monometallic sample. These results indicate, at first place, that the high CO conversion observed in the WGS reaction on monometallic Ni catalyst could be caused by an important contribution of the CO methanation reaction at high temperatures. Similar behavior was previously reported for Ni/SiO_2 [32], Ni/CeO_2 [33], Ni/Al_2O_3 [34] and Ni/ZrO_2 [35] catalysts, in good agreement with the data presented in this paper. Contrary to its Ni analogue, Cu monometallic sample was completely inactive in the methanation reaction. When Cu-Ni samples were tested, a strong effect of the Cu incorporation on the CH_4 yield was observed. Analogously to the gasification reaction, the presence of Cu attenuates Ni methanation activity. Very recently, Saw et al. [24] observed a similar behavior over $Cu\text{-}Ni/CeO_2$ catalysts and attributed the suppression of the methanation activity to the Cu- Ni alloy formation and its influence on the CO adsorption behavior and dissociation ability. Not only the alloying could suppress the Ni methanation activity, for example, a decrease by Na addition of the low coordinated Ni atoms, responsible for the CO breaking and subsequent hydrogenation reaction could also account for this [36]. However, as observed for our samples, the quantity of the introduced Cu does not seem to affect the methanation activity. For both bimetallic samples, the CH_4 yields decrease in the same range is observed. Nevertheless the difference of the CO oxidation activity for the both samples should be taken into consideration the lower CO conversion of the Cu-Ni:1-2/AC could induce also lower CH_4 formation and masques an Cu loading influence on the methanation reaction. Besides, very interestingly, Cu-Ni:2-1/AC catalyst showed similar activity in methanation, like the reported for $Cu\text{-}Ni/CeO_2$ [26] under

similar reaction conditions, suggesting that the observed effect should be attributed only to the metallic phase.

Going back to the WGS activity, it is clear that Cu-Ni ratio of 2 maintains the high activity of the Ni based catalysts without spending H_2 for methane formation. However, the decrease of the Cu-Ni ratio to 0.5 does not show any beneficial effect on the activity. It seems that the WGS activity increases with the metals synergy favored in copper rich alloys.

Additionally, all the catalysts were tested in realistic WGS mixture (Table 1) at 350 °C and the CO conversion is presented in Figure 3 in comparison to the equilibrium value for this temperature. Slightly higher CO conversion than the equilibrium one is observed due to the formation of CH_4 at this temperature, as shown in Figure 2.

Although the observed CH_4 formation the superiority of the Cu-Ni:2-1/AC bimetallic catalysts under realistic WGS conditions is clearly evidenced. Even more important gap is opened between the samples performances in realistic conditions suggesting a special active sites arrangement for the Cu-Ni:2-1/AC catalyst.

3.1.2 Stability of the catalyst

A long term stability test of the most active sample (Cu-Ni:2-1/AC) is presented in Figure 4. The reaction was carried out at 330 °C under realistic mixture conditions (Table 1), a temperature selected to start at non-equilibrium CO conversion high enough to observe the deactivation of the catalyst.

The CO conversion decreases continuously from 65% to 28 %. The activity drop mainly occurs during the initial hours. After that, the catalyst appears to reach the steady state and maintains a

stable conversion during 20 hours of reaction. Several reasons for this deactivation could be enumerated. Firstly, the formation of carbonaceous deposits over the Ni based catalysts through CO dissociation via Boudouard reaction, previously reported by Flaherty *et al.* [37] and Wu *et al*. [38]. However the presence of copper, in principle, should mitigate this deactivation. Experiences reported by Yang *et al*. [39], show that carbon formation does not occur over Cu monometallic catalysts. On the other hand, the WGS reaction could proceed through the formation of COH* species strongly attached to the catalyst surface causing the loss of active sites and therefore catalytic activity [40]. To elucidate whether the formation of some carbonaceous species occurs during water gas shift, a temperature programmed desorption post-reaction experiments were performed and discussed below.

3.1.3 Start/stop cycles stability

A suitable catalyst for practical applications must withstand start/stop cycles. For instance, the use of a WGS unit in an integrated fuel processor is submitted to continuous start-up/shutdowns of the engine thus the WGS catalysts must be robust enough in this regard. Therefore, the bimetallic Cu-Ni:2-1/AC catalyst was submitted to several cycles (Figure 5). The series of cycles were carried out by cooling the system until room temperature. Once the system reaches this temperature the reaction feed was passed through the catalytic bed during 30 min and heated again to the chosen temperature (330 ºC). The later provides the conditions to water condensation in the pores of the catalyst and in the catalytic bed. Because of the presence of liquid water, this test is considered as one of the most demanding resistance test for the WGS catalysts [41].

The experimental results revealed that Cu-Ni:2-1 catalyst maintains its catalytic activity in these conditions. CO conversion at about 55% during all start/stop cycles without any significant deactivation observed. Furthermore, a slight increase of the CO conversion was detected in the first cycles. The reason of this activity improvement is related to the exothermicity of the reaction and the rapid increase of the temperature when the reaction starts. The excess of condensed water in the catalytic bed accounts for a virtual "pre-ignition" regime which boosts the conversion due to the rapid vaporization and the high amount of water in contact with CO at high temperature. The experimental results showed that this catalyst appears to be more stable than Cu−Al_2O_3-$CuAl_2O_4$ [42] for which an activity loss of about 30% after the first stop/start cycle using similar feed gas is reported. For all exposed above, it could be concluded that very active and robust Cu-Ni based catalysts can be obtained and presented as a suitable candidate to compete with the already available noble metal based systems operating in this temperature range with similar performance and standing of the start/stop cycles.

3.2 Catalyst characterization

For understanding the differences in catalytic behavior exhibited by the prepared samples several characterization techniques were employed.

3.2.1 XRD diffraction results

The XRD patterns of the mono and bimetallic reduced copper-nickel catalysts are shown in Figure 6.

For all the samples the corresponding oxide phases were not detected. The monometallic Cu/AC and Ni/AC samples present a diffraction pattern corresponding to the metallic (Ni or Cu) fcc cell with the most intensive diffractions located at 2θ = 43.3˚ (111) and 50.4˚ (200) for Cu (JCPDS# 4-0836) and 2θ = 44.5˚(111), 51.8˚ (200) for Ni^0(JCPDS# 4-0850). Both metals present a complete solubility at the studied temperatures allowing the formation of the solid solution. Indeed, for the bimetallic samples Cu-Ni:2-1/AC and Cu-Ni:1-2/AC samples, the diffraction lines corresponding to (111) and (200) shift linearly with the Cu loading increase. The increase of the lattice parameter as a function of the Cu concentration agrees with the Vegard's law (Figure 6 inset) and indicates the formation of a Cu-Ni alloy in this composition range. The formation of the Cu-Ni alloy may account for the diminished methanation and suppressed gasification activity of the bimetallic samples during the reaction, as reported elsewhere [24]. In addition, Cu and Ni as well as both alloys particle sizes were estimated using Scherrer equation (Table 3). Interestingly, the bimetallic samples presented smaller particle size than the monometallic systems. It is well known that on relatively small particles, the fraction of defect sites, e.g. corner sites and low coordination atomic sites is higher than for relatively large particles, and thus small particles exhibit higher number of adsorption sites and thus higher catalytic activity. In any case, the bimetallic systems are composed for smaller and well dispersed metallic particles contributing for the better WGS behavior.

3.2.2 BET measurements and X-Ray microfluorescence spectrometry results

Figure 7 shows the N_2 adsorption−desorption isotherms of all the samples. No significant changes in the textural properties of bimetallic catalyst in comparison to the monometallic were

observed indicating similar surface area (see Table 3). All isotherms are of type IV with hysteresis loops (IUPAC classification H4), which are usually observed for mesoporous solids with slit-shaped pores of non-uniform sizes and shapes, and important contribution of mesopores (2 nm<pore size<50 nm) such as is shown in Table 3.

Table 3. Surface area and pore volume of tested catalysts

Catalyst	Surface area (m^2/g)	Pore size (nm)	Cu content (wt.%)	Ni content (wt.%)	Actual Cu-Ni molar ratio	[1]Metal particle size (nm)
AC	503	4.2	---	---	---	---
Cu	419	2.9	100	---	---	25.4
Ni	417	2.8	---	100	---	22.3
Cu-Ni:2-1	415	3.1	62.7	37.3	1.56	13.7
Cu-Ni:1-2	434	2.9	35.7	64.3	0.51	13.2

[1]Estimated using Scherrer equation from (111) and (200) reflexions.

The metal addition causes a decrease of the pore size but without defined trend. Surface area of mono and bimetallic catalysts are lower than the surface area of the activated carbon pellets (503 m^2/g). BET surface area measurements (Table 3) indicate that the addition of the metals (Cu and Ni) on the support resulted in a decrease of the surface area, as a consequence of insertion of the active phase in the pores of the support.

For the Cu/Ni:2/1/AC catalyst lower actual metal loading is obtained a loss of Cu is detected, contrary to the Cu/Ni:1/2/AC where the nominal value is obtained.

3.2.4 TPD measurements

The species formed during the WGS on the catalysts surface after testing in realistic conditions were monitored by several post-reaction TPD experiments. The evolution of mass signals m/z = 2, 18, 28 and 44 corresponding to H_2, H_2O, CO and CO_2 and the decomposition temperature of various surface groups in both monometallic and Cu-Ni:2-1/AC bimetallic catalyst are presented in Figure 8. The TPD profile of the bimetallic Cu-Ni:2-1/AC sample before the reaction is also included for comparison.

The TPD profile of the pre-reaction sample evidences the desorption of CO and H_2 at high temperatures (above 500 ºC), signals most likely related to the decomposition of some functional groups of the activated carbon support surface. In fact, all the post-reaction samples presented a similar profile in the high temperature range exhibiting CO and H_2 desorption. The latter makes difficult the discrimination among desorption of the species formed during the reaction and the signals caused by the support, at least at high temperatures. Actually, only the Cu/AC sample presents a slightly different desorption profile at high temperatures where CO and H_2 signals seem to evolve together simultaneously. For the rest of the samples CO desorption occurred before that of H_2. However in the low temperature range H_2O and CO_2 desorption are the most significant signals and minute but interesting differences between the catalysts can be noticed. In particular, the CO_2 profile is worth to analyze. The pre-reaction sample released all the CO_2 before 500 ºC while the spent catalysts showed carbon dioxide signals above 600 ºC. This observation reveals that a part of CO_2 desorption is due to carbonaceous species formed during

the WGS. These species require high temperatures to be removed from the catalysts surface and they are accumulated during the reaction probably blocking the active sites of the catalyst surface. This blocking phenomenon could explicate the loss of activity observed in the stability test previously discussed. It must be mentioned that the Ni/AC catalysts is the one that accumulates more carbonaceous species in view of the broad CO_2 signal presented in this solid ranging from 180 to 800ºC. The Cu/AC systems seems to accumulate less quantity of carbonaceous species but they seem to be strongly attached since the desorption occurs up to 900 ºC. Nevertheless, the most active catalysts Cu-Ni:2-1/AC is the one that concentrates less amount of blocking species, in other words, this is the sample with higher concentration of available actives sites, in good agreement with its superior activity.

3.2.5. Temperature programmed reduction TPR analyses

In order to study the re-oxidation behavior of the samples, the as prepared reduced pre-reaction samples were submitted to TPR analysis. The H_2 consumption of the samples compared to the theoretical consumption is presented in Table 4. The % of reoxidation was calculated as the relation between the theoretical and experimental H_2 consumption.

Table 4. H_2 consumption of the pre-reaction catalysts

Catalyst	Cu	Ni	Cu-Ni:2-1	Cu-Ni:1-2
Theoretical H_2 consumption mmol H_2/g cat.	2.5	2.67	2.69	2.22
Experimental H_2 consumption mmol H_2/g cat.	0.29	0.34	0.4	0.21
Re-oxidation %	11.6	12.7	14.9	9.4

The results indicate that the Cu-Ni:2-1 sample appears to be the most easily oxidized sample during the catalyst storage. The TPR profiles of the samples are presented in Figure 9. All the samples present broad hydrogen consumption at high temperature (> 500 °C) associated to the partial gasification of carbon support (observable also in activated carbon) with the formation of CH_4 due the reaction of C and H_2. However this hydrogen consumption does not influence the samples during the WGS activity being outside of the reaction window.

The most significant differences are observed in the low to medium temperature range of reduction. The TPR profile of the Cu monometallic catalyst exhibits a main reduction peak at 251°C attributed to oxidized copper reduction, either CuO or Cu_2O. The TPR profile of Ni monometallic catalyst sample shows two zones of reduction, the first one centered at 281°C with a shoulder at 242°C attributed to the reduction of NiO particles with different dispersion. The second zone centered at 380°C could be due to the reduction of free NiO cluster with a weak interaction with the support [43] formed during the thermal treatments.

For the bimetallic samples, a broad peak centered at 237 and 228 °C are observed for the Cu-Ni:2-1/AC and Cu-Ni:1-2/AC samples, respectively. The reduction profiles of the bimetallic samples follow the same tendency than the monometallic samples, being proportional to the dominant metal, e.g. the Ni rich catalyst (Cu-Ni:1-2) profile resembles that of the Ni/AC sample and the Cu-rich one (Cu-Ni:2-1) is similar to that of the Cu/AC sample. Nevertheless, the presence of the second metal improves of the reducibility in terms of reduction temperature diminution, compared to the monometallic oxide samples, an effect previously demonstrated for the Cu-Ni/SiO_2 catalysts [42]. The synergy of copper and nickel oxides is evidenced also by the TPR profiles and simultaneously could be correlated with the WGS activity. Therefore,

according to the TPR profiles Cu is completely reduced in the reductive activation at 350°C and should remain Cu^0 during the WGS. Nevertheless, a part of Ni could remain oxidized (see the second reduction process of Ni in the profiles above 350ºC).

3.2.6 X-ray photoelectron spectroscopy analyses

To study the initial state of our monometallic Cu/AC, Ni/AC and bimetallic Cu-Ni:2-1/AC samples an XPS study was carried out. Figure 10 represents Cu 2p for both, Cu monometallic and Cu-Ni:2-1 bimetallic samples. It is well known that the analysis of Cu 2p spectrum allows unambiguously distinguishing between Cu^{2+} and Cu^{1+} / Cu^0 cations.

The Cu monometallic catalyst exhibits XP spectra with Cu $2p_{3/2}$ and Cu $2p_{1/2}$ main peaks appearing around 932.8 and 952.8 eV, respectively with a spin–orbit coupling energy of 20.0 eV and two strong satellite speaks (marked as "shake-up" in the figure) at 944.2 and 962.6 eV (Table 5) [44], [45] According to the literature data [46] the Cu metal and Cu_2O are characterized by the $Cu2p_{3/2}$ binding energy in the range of 932.4-932.8 eV, while the binding energy for CuO is between 933.6 and 934.6 eV. Moreover, the Cu 2p spectra of different Cu^{2+} compounds are characterized by high-intensity shake-up satellites at 9 to12 eV higher binding energy of the main Cu $2p_{3/2}$ and Cu $2p_{1/2}$ peaks, whereas these satellites are absent in the spectra of metallic copper and Cu_2O. The shape of the Cu 2p spectra of the catalysts under study indicates that copper is present in Cu^{2+} at least at the surface layers. However from the asymmetry of the peaks the contribution of Cu^0 and/or Cu^{1+} states could be perceived. The TPR

of those samples showed only 10-15% of re-oxidation of the surface which confirms the XPS results according to which the surface layers are oxidized.

Some significant differences in the position and intensities of the peaks are observed in the spectra of the bimetallic catalysts. The peak positions are shifted towards higher binding energy in comparison to that of the monometallic catalyst. Moreover, a decrease in intensity of satellite peaks in the bimetallic catalysts was observed. The results indicate that the Cu^{2+} in the monometallic system becomes partially reduced when is mixed with the Ni. The decrease of the satellite peak in the Cu:Ni-2:1/AC bimetallic catalyst indicates the reduction of Cu^{2+} to Cu^{1+} or metallic state (Cu^0). Both Cu^{1+} and Cu^0 should have the same binding energy in the core level XPS, therefore, with this technique is not possible to distinguish the two oxidation states of Cu (Cu^0 or Cu^+) [47]. However crossing this information with the TPR where higher reoxidized fraction was observed for this sample at least 15 % of the species should be Cu^+ species, which are presumably reduced before starting the WGS reaction. Nevertheless taking in account the high oxidation ability of water the presence of these species could not be excluded during the WGS reaction.

Table 5. Cu 2p and Ni 2p XPS parameters for mono and bimetallic catalysts.

Catalyst	Cu $2p_{3/2}$ (eV)	Cu $2p_{1/2}$ (eV)	ΔE (eV)	Ni $2p_{3/2}$ (eV)	Ni $2p_{1/2}$ (eV)	ΔE (eV)	At.%
Cu/AC	932.8	952.8	20.0	-	-	-	7.5
Cu-Ni/AC-2-1	933.1	953.1	20.0	856.3	873.9	17.6	2.4(Cu) 1.5(Ni)
Ni	-	-	-	854.1	872.6	18.5	15.6

The Ni 2p core level XP spectra for mono and bimetallic catalysts are shown in Figure 11. The monometallic catalyst exhibits an intense doublet centered at 854.1 eV and 872.6 eV, and attributed to Ni 2 $p_{3/2}$ and Ni 2 $p_{1/2}$, respectively with a spin-orbit coupling energy of 18.5 eV and low-intensity satellites associated to the energy loss peaks due to the plasmon excitation of the metal [48]. The literature reports Ni 2 $p_{3/2}$ binding energy in the range of 852.4-853.0 eV for the Ni metal state and in the range of 854.5-856.6 eV for NiO [48]. The analysis of the Ni 2p spectra points out that Ni in the mono and bimetallic catalysts exists mainly in oxidized state at least in the surface and subsurface layers. Nevertheles for the bimetallic catalyst Ni $2p_{3/2}$ binding energy shift to higher binding energy, and similar positive shift is observed also for Cu $2p_{3/2}$ for this sample.

Although the determination of the Cu-Ni alloy formation by XPS is difficulted by the fact that the d- and sp- electron occupation is complicated by the relative participation of the Fermi energy, the relaxation or screening of the final state and the potential parameters [47] a positive shift in the binding energy of both Ni and Cu species (0.2-0.3eV) is normally reported as an evidence to strong metallic interaction or formation of Cu-Ni alloy [49].

As for the surface chemical composition (Table 5), the data indicate Cu/Ni surface concentration of 1,6 in agreement with that found by the elemental analysis and suggesting surface and bulk homogeneous composition, which is also indication of Cu-Ni alloy formation, as observed by XRD .

As described above, Saw et al. [24] found in their study a Cu-Ni molar ratio of 1 as optimal for excellent catalytic properties. Although this ratio is not considered in this study it is clear that the Ni-rich catalyst behaves worst that the Cu-rich ones. As for the active sites, in the bimetallic Cu-Ni:2-1/AC catalyst besides the existence of the Cu-Ni alloy confirmed by XRD and XPS the

presence of water could induce partial oxidation of both metals, being Ni and Cu rapidly oxidized metal but the former present lower rate of reduction in comparison to Cu. The later could imply the existence of Cu^0/NiO_x interface. The electronic interchange between those phases could provide an electron rich interface where the reactant molecules can be activated and the reaction favored. Nevertheless additional studies are needed to confirm this supposition.

4. CONCLUSIONS

Pelletized monometallic Cu and Ni and bimetallic Cu-Ni:2-1/AC and Cu-Ni:1-2/AC catalysts supported on activated carbon were synthesized and evaluated in the water gas shift reaction. It was found that the catalytic activity (in terms of CO conversion) increases with increasing of the reaction temperature for all tested samples, being the Cu-Ni:2-1/AC the most active sample (99.4% CO conversion). Additionally, this sample exhibited lower methanation activity and suppresses the carbon gasification reaction. The improved catalytic activity was related to the formation of Cu-Ni alloy evidenced by XRD and or to a possible Cu/NiOx active site formation. The synergy between Cu and Ni accounts for the suppression of the methanation activity, observed for the Ni catalyst. This work offers a very promising candidate for the medium temperature WGS from economical point of view. The Cu-Ni:2-1/AC pelletized catalyst presents comparable performance to the noble metal ceria supported catalysts in the studied temperature range with the advantage of cheaper support and active phase. Although an excellent performance of the catalyst in the start/stop cycles was observed the long term stability of the catalyst should be improved. All of these catalytic skills, together with their economic feasibility

and their relatively easy preparation make these catalysts an interesting alternative for the pure hydrogen production directed towards fuel cell applications.

5. ACKNOWLEDGMENTS

The authors would like to thank, the Universidad de Antioquia for financial support of this work by Sustainability Strategy 2013-2014. T. R. Reina acknowledges CSIC for his JAE-Predoc fellowship cofinanced with the European social program and S. Ivanova MEC for her Ramon y Cajal contract. The authors thank to Spanish Ministerio de Economia y Competitividad (MINECO) ENE2013-47880-C3-2-R

REFERENCES

[1] B. Dou, Y. Song, C. Wang, H. Chen, Y. Xu, Renew. Sustain. Energy Rev. 30 (2014) 950-960.

[2] U. Lucia, Renew. Sustain. Energy Rev. 30 (2014) 164-169.

[3] C. Oettel, L. Rihko-Struckmann, K. Sundmacher, Int. J. Hydrogen Energy 37 (2012) 6635-6645.

[4] R. Chaubey, S. Sahu, O.O. James, S. Maity, Renew. Sustain. Energy Rev. 23 (2013) 443-462.

[5] O.H. Laguna, W.Y. Hernández, G. Arzamendi, L.M. Gandía, M. A. Centeno, J. A. Odriozola, Fuel 118 (2014) 176-185.

[6] M.M. Zyryanova, P.V. Snytnikov, R.V. Gulyaev, Y.I. Amosov, a. I. Boronin, V. a. Sobyanin, Chem. Eng. J. 238 (2014) 189-197.

[7] R. Costa Neto, I. Monteiro, R. Maximino, J.T. De Azevedo, Int. J. Hydrogen Energy 39 (2014) 5242-5247.

[8] S. Colussi, L. Katta, F. Amoroso, R.J. Farrauto, A. Trovarelli, Catal. Commun. 47 (2014) 63-66.

[9] L. Bollmann, J. Ratts, a Joshi, W. Williams, J. Pazmino, Y. Joshi, J. Miller, a Kropf, W. Delgass, F. Ribeiro, J. Catal. 257 (2008) 43-54.

[10] R. Watanabe, Y. Fujita, T. Tagawa, K. Yamamoto, T. Furusawa, C. Fukuhara, Appl. Catal. A Gen. 477 (2014) 75-82.

[11] K.-R. Hwang, S.-K. Ihm, S.-C. Park, J.-S. Park, Int. J. Hydrogen Energy 38 (2013) 6044-6051.

[12] P. Panagiotopoulou, D.I. Kondarides, Appl. Catal. B Environ. 101 (2011) 738-746.

[13] R. Jain, R. Maric, Appl. Catal. A Gen. 475 (2014) 461-468.

[14] J. A. Rodriguez, Catal. Today 160 (2011) 3-10.

[15] B. A. Lenite, C. Galletti, S. Specchia, Int. J. Hydrogen Energy 36 (2011) 7750-7758.

[16] K.G. Azzam, I.V. Babich, K. Seshan, L. Lefferts, Appl. Catal. A Gen. 338 (2008) 66-71.

[17] A. A. El-Moemen, G. Kučerová, R.J. Behm, Appl. Catal. B Environ. 95 (2010) 57-70.

[18] I. Yati, M. Ridwan, G.E. Jeong, Y. Lee, J.-W. Choi, C.W. Yoon, D.J. Suh, J.-M. Ha, Catal. Commun. 56 (2014) 11-16.

[19] J. Kugai, J.T. Miller, N. Guo, C. Song, J. Catal. 277 (2011) 46-53.

[20] T.R. Reina, E. Papadopoulou, S. Palma, S. Ivanova, M. a. Centeno, T. Ioannides, J. A. Odriozola, Appl. Catal. B Environ. 150-151 (2014) 554-563.

[21] B.V. Farahani, F.H. Rajabi, M. Bahmani, M. Ghelichkhani, S. Sahebdelfar, Appl. Catal. A Gen. 482 (2014) 237-244.

[22] J. Bian, X.W. Wei, Y.R. Jin, L. Wang, D.C. Luan, Z.P. Guan, Chem. Eng. J. 165 (2010) 686-692.

[23] O. Arbeláez, A. Orrego, F. Bustamante, A.L. Villa, Top. Catal. 55 (2012) 668-672.

[24] E.T. Saw, U. Oemar, X.R. Tan, Y. Du, a. Borgna, K. Hidajat, S. Kawi, J. Catal. 314 (2014) 32-46.

[25] A.R.S. Rad, M.B. Khoshgouei, S. Rezvani, A.R. Rezvani, Fuel Process. Technol. 96 (2012) 9-15.

[26] J.H. Lin, V. V. Guliants, Appl. Catal. A Gen. 445-446 (2012) 187-194.

[27] D. Jeong, W.-J. Jang, J.-O. Shim, W.-B. Han, H.-S. Roh, U.H. Jung, W.L. Yoon, Renew. Energy 65 (2014) 102-107.

[28] C. Chen, C. Ruan, Y. Zhan, X. Lin, Q. Zheng, K. Wei, Int. J. Hydrogen Energy 39 (2014) 317-324.

[29] J.L. Figueiredo, M.F.R. Pereira, Catal. Today 150 (2010) 2-7.

[30] A.C. Chien, S.S.C. Chuang, J. Power Sources 196 (2011) 4719-4723.

[31] M.P. Andersson, F. Abild-Pedersen, I.N. Remediakis, T. Bligaard, G. Jones, J. Engbæk, O. Lytken, S. Horch, J.H. Nielsen, J. Sehested, J. Catal. 255 (2008) 6-19.

[32] M. A. A. Aziz, a. a. Jalil, S. Triwahyono, R.R. Mukti, Y.H. Taufiq-Yap, M.R. Sazegar, Appl. Catal. B Environ. 147 (2014) 359-368.

[33] S. Tada, T. Shimizu, H. Kameyama, T. Haneda, R. Kikuchi, Int. J. Hydrogen Energy 37 (2012) 5527-5531.

[34] J. Gao, C. Jia, J. Li, M. Zhang, F. Gu, G. Xu, Z. Zhong, F. Su, J. Energy Chem. 22 (2013) 919-927.

[35] C. Guo, Y. Wu, H. Qin, J. Zhang, Fuel Process. Technol. 124 (2014) 61-69.

[36] M.L. Ang, U. Oemar, E.T. Saw, L. Mo, Y. Kathiraser, B.H. Chia, S. Kawi, ACS Catal. 4 (2014) 3237-3248.

[37] D.W. Flaherty, W.-Y. Yu, Z.D. Pozun, G. Henkelman, C.B. Mullins, J. Catal. 282 (2011) 278-288.

[38] Y. Wu, C. Su, C. Zhang, R. Ran, Z. Shao, Electrochem. Commun. 11 (2009) 1265-1268.

[39] Y. Yang, C. A. Mims, D.H. Mei, C.H.F. Peden, C.T. Campbell, J. Catal. 298 (2013) 10-17.

[40] X. Liu, P. Guo, B. Wang, Z. Jiang, Y. Pei, K. Fan, M. Qiao, J. Catal. 300 (2013) 152-162.

[41] R.J. Farrauto, Y. Liu, W. Ruettinger, O. Ilinich, L. Shore, T. Giroux, Catal. Rev. 49 (2007) 141-196.

[42] O. Ilinich, W. Ruettinger, X. Liu, R. Farrauto, J. Catal. 247 (2007) 112-118.

[43] L.F. Bobadilla, S. Palma, S. Ivanova, M.I. Domínguez, F. Romero-Sarria, M. A. Centeno, J. A. Odriozola, Int. J. Hydrogen Energy 38 (2013) 6646-6656.

[44] S.P. Patil, J. V. Pande, R.B. Biniwale, Int. J. Hydrogen Energy 38 (2013) 15233-15241.

[45] A. Corma, A. Palomares, F. Márquez. J. Catal. 170 (1997) 132-139.

[46] J. Morales, L. Sánchez, F. Martín, J.R. Ramos-Barrado, M. Sánchez, Thin Solid Films 474 (2005) 133-140.

[47] P. Barbieri, A de Siervo, M. Carazzolle, R. Landers, G. Kleiman, J. Electron Spectros. Relat. Phenomena 135 (2004) 113-118.

[48] S. A. Khromova, A. A. Smirnov, O. A. Bulavchenko, A. A. Saraev, V. V. Kaichev, S.I. Reshetnikov, V. A. Yakovlev, Appl. Catal. A Gen. 470 (2014) 261-270.

[49] H. Wei, K. Xie, J. Zhang, Y. Zhang, Y. Wang, Y. Qin, J. Cui, J. Yan, Y. Wu, Sci. Rep. 4 (2014) 1-11.

Graphical abstract

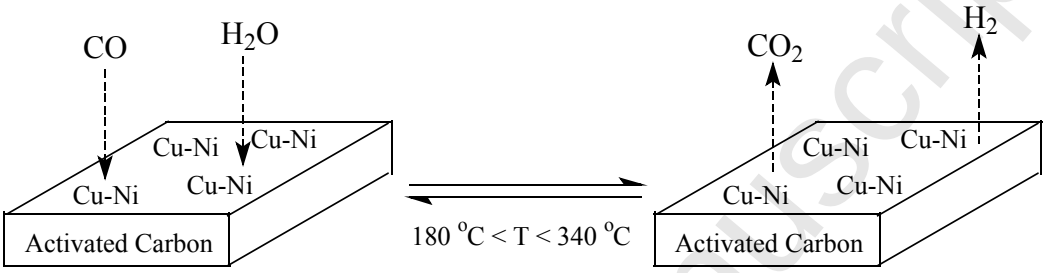

Figure 1. WGS activity of the tested catalysts in model mixture.

Figure 2. CH_4 yield (%) of the tested catalysts in methanation reaction.

Figure 3. CO conversion in realistic WGS conditions at temperature of 350° C.

Figure 4. WGS stability on Cu-Ni:2-1 catalyst at 330° C in realistic conditions.

Figure 5. Start –stop cycles at 330°C in realistic conditions.

Figure 6. XRD of mono and bimetallic catalysts.

Figure 7. Adsorption-desorption isotherms of N_2 on Cu-Ni supported on activated carbon samples.

Figure 8. TPD profiles of the selected samples.

Figure 9. TPR profiles for pelletized monometallic and bimetallic tested catalysts.

Figure 10. XPS analysis of Cu 2p of Cu monometallic and Cu:Ni-2:1 bimetallic catalyst.

Figure 11. XPS analysis of Ni 2p of Ni monometallic and Cu:Ni-2:1 bimetallic catalyst.

Figure 1

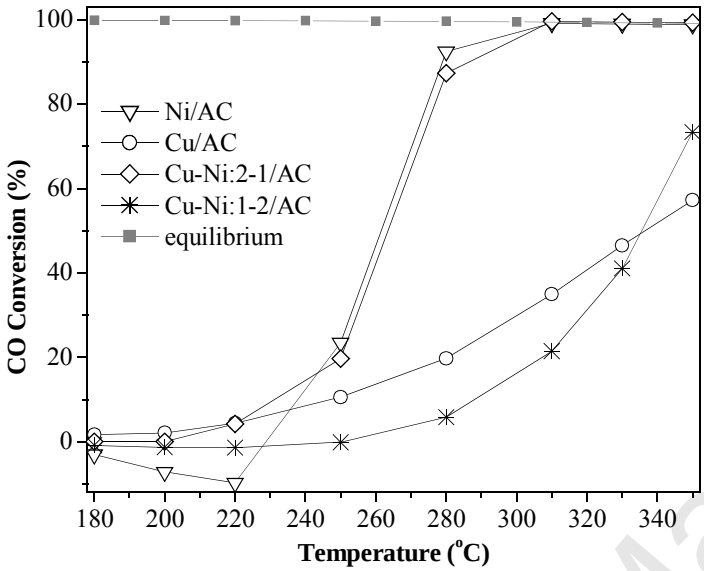

Figure 2

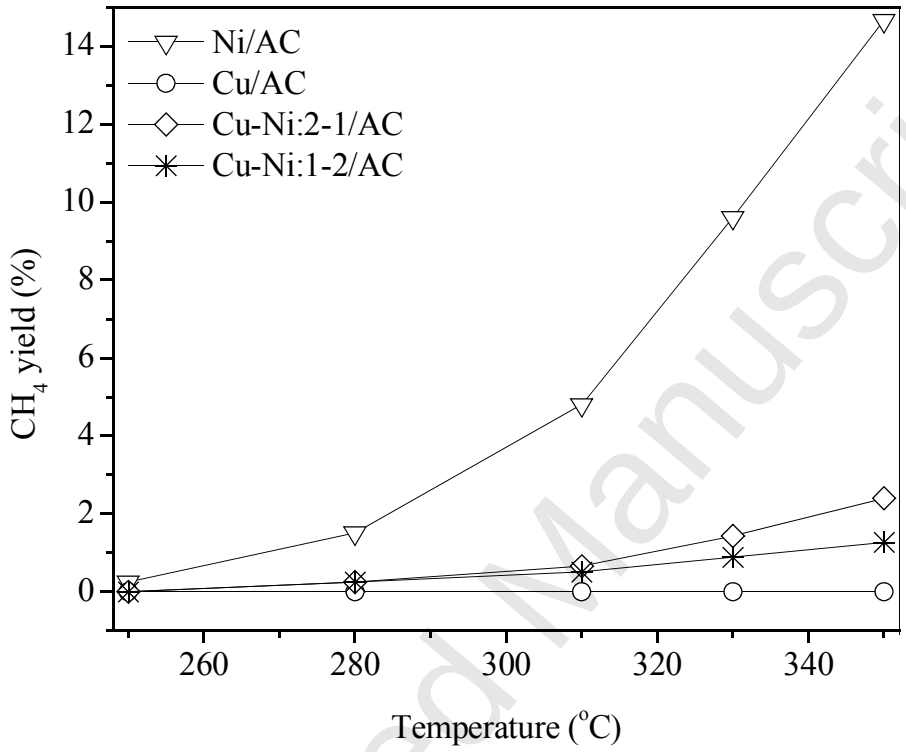

Figure 3

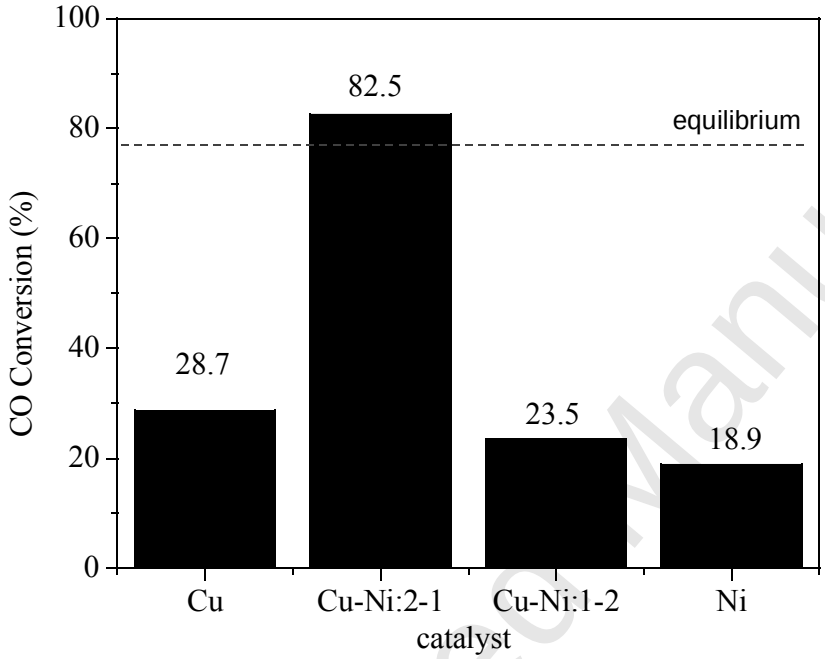

Figure 4

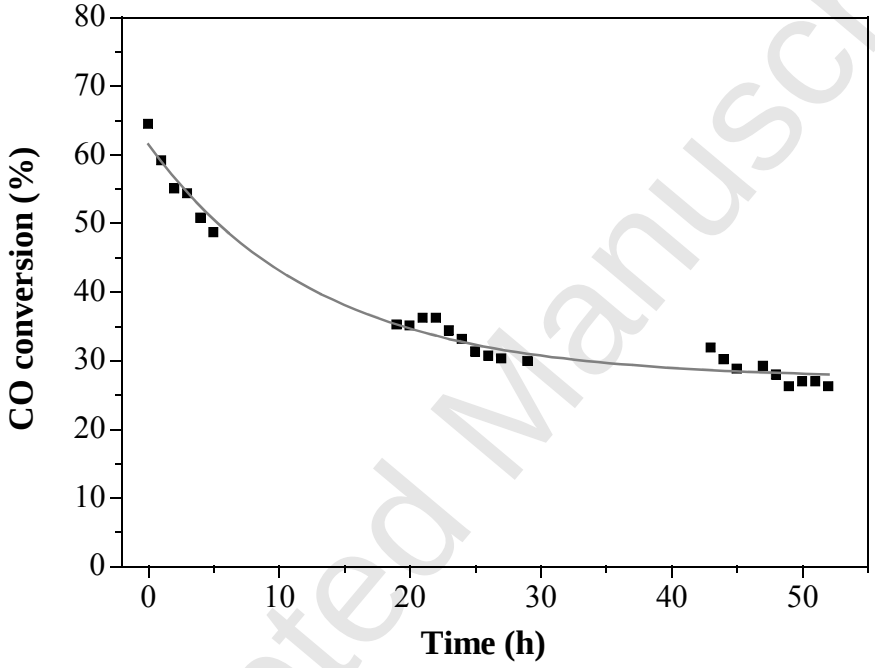

Figure 5

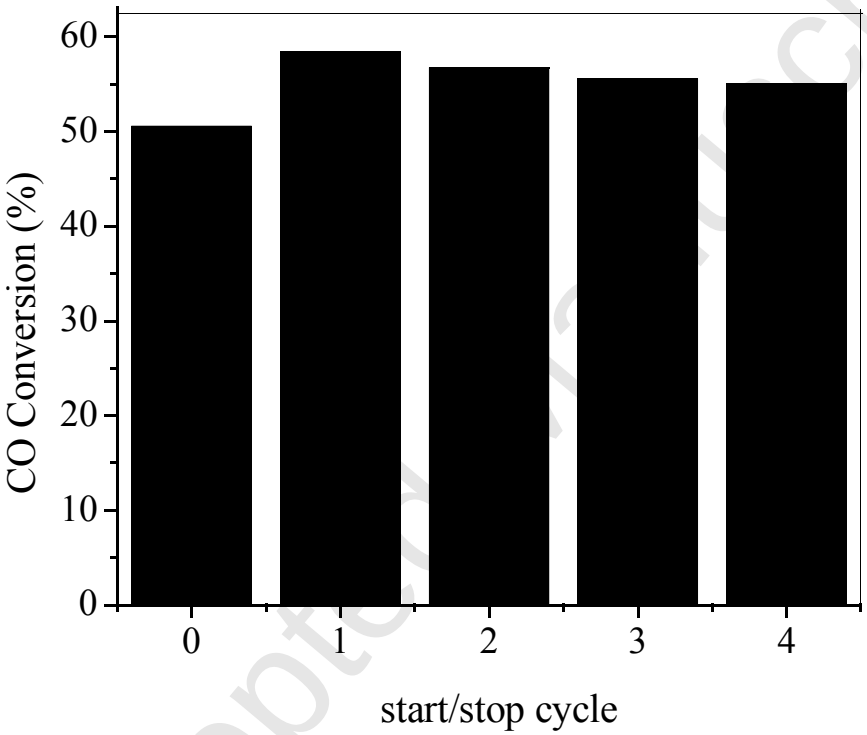

Figure 6

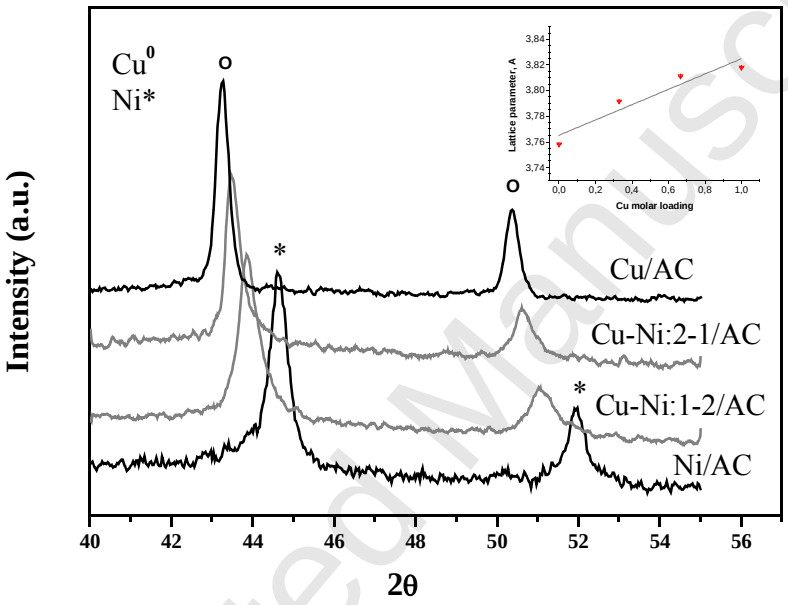

Figure 7

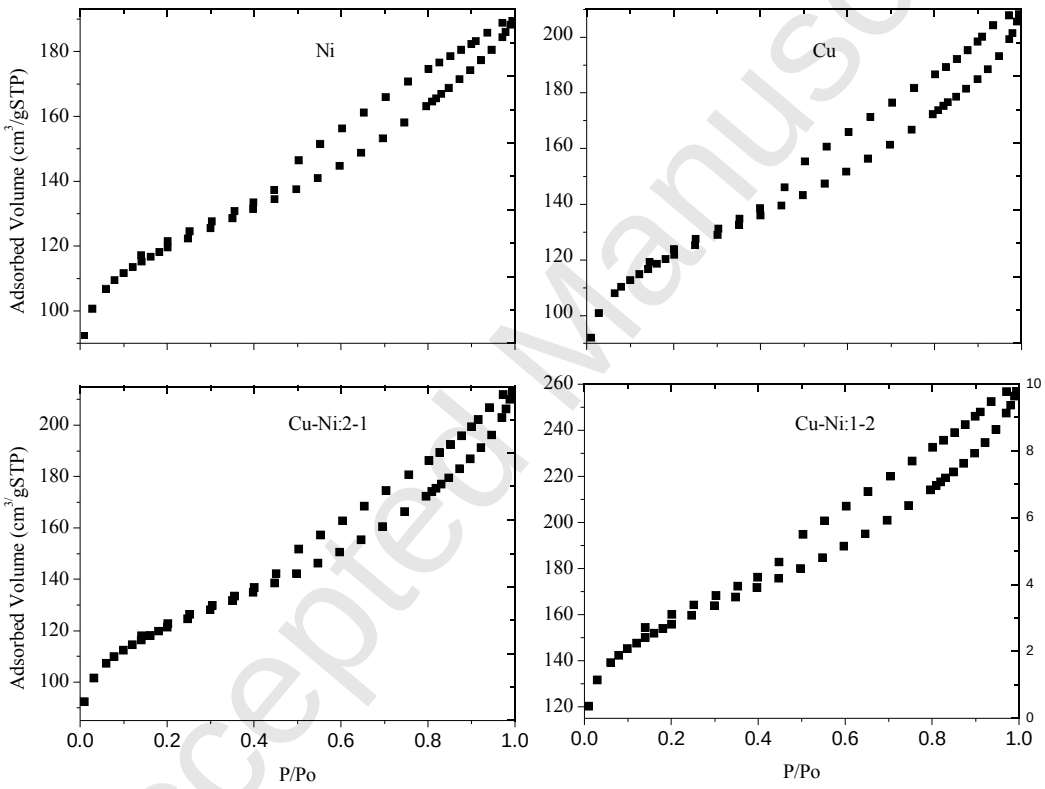

Figure 8

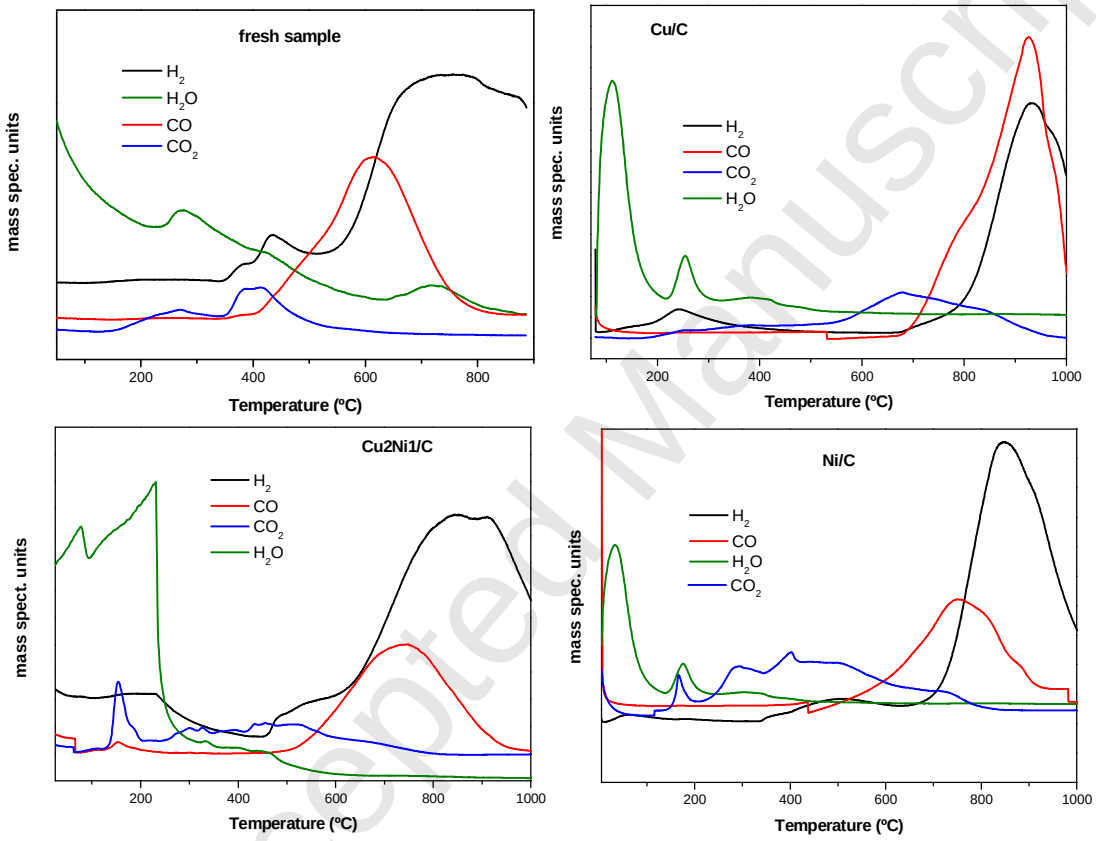

Figure 9

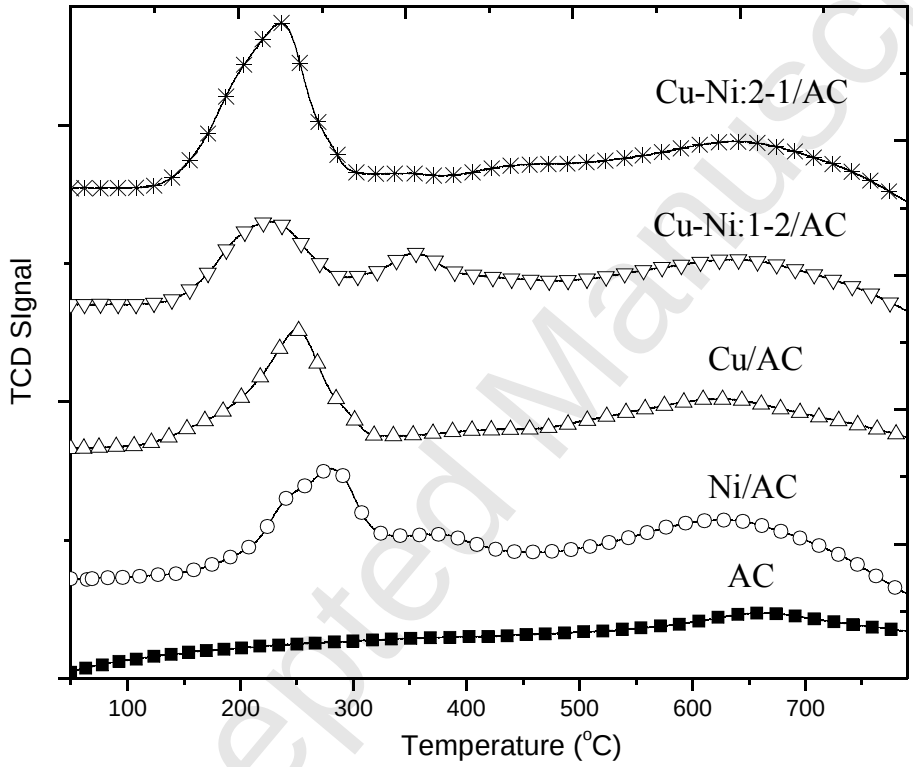

Figure 10

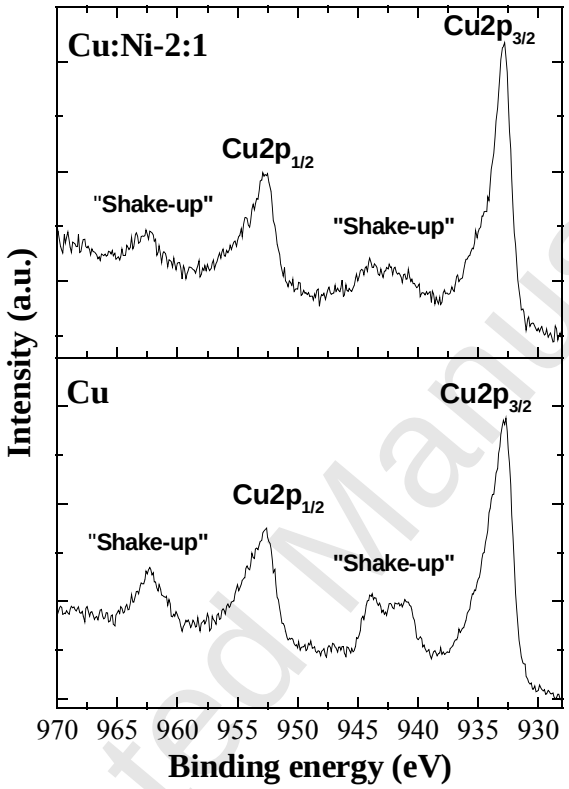

Figure 11